A Detailed Study of Thermal, Hydrothermal, and Mechanical Stabilities of a Wide Range of Surfactant Assembled Mesoporous Silicas

K. Cassiers,* T. Linssen, M. Mathieu, M. Benjelloun, K. Schrijnemakers, P. Van Der Voort, P. Cool, and E. F. Vansant

Department of Chemistry, Laboratory of Adsorption and Catalysis, University of Antwerp, Universiteitsplein 1, B-2610 Wilrijk, Belgium

Received November 28, 2001. Revised Manuscript Received February 19, 2002

The thermal, hydrothermal, and mechanical stabilities of a wide range of ordered mesoporous materials, in particular, the molecular sieves MCM-41, MCM-48, HMS, FSM-16, KIT-1, PCH, and SBA-15, have been studied in detail using X-ray diffraction (XRD) and nitrogen sorption. The thermal stability was found to be strongly related to the wall thickness and the silica precursor used during synthesis, and the following stability trend was observed: MCM-41 (fumed silica), MCM-48 (fumed silica), KIT-1 (colloid silica) > SBA-15 (TEOS) > FSM-16 (layered silicate), PCH (layered silicate) > MCM-41 (TEOS), MCM-48 (TEOS), HMS (TEOS). The hydrothermal stability is influenced by the wall thickness and the polymerization degree and decreases according to the following trend: KIT-1 > SBA-15 > MCM-48 (fumed silica and TEOS), PCH > FSM-16, MCM-41 (fumed silica and TEOS), HMS. The mechanical stability is little influenced by the nature of the mesoporous molecular sieves. All materials collapsed at a maximum pelletizing pressure of 450 MPa.

Introduction

The family of highly ordered mesoporous siliceous materials, designated as M41S (MCM-41 and MCM-48), has attracted a great deal of attention as new potential molecular sieves and supporting materials.[1,2] Parallel to the development of M41S materials, many other ordered mesophases with similar properties have been synthesized (e.g., HMS,[3,4] FSM-16,[5] PCH,[6] SBA,[7] MSU,[8] and KIT[9]). Several research groups have reported successful applications of these semicrystalline silica zeolites. Mesostructured silicas with incorporated or grafted transition metals have been reported to have outstanding catalytic activities because the porous network facilitates mass transfer of reactants to the catalytic sites.[4,10] The presence of large and tunable uniform pores (15−100 Å) opens up the possibility for shape-selective conversions of bulky molecules and pharmaceutical products.[11] Furthermore, surface-modified mesoporous molecular sieves might find other potential applications, such as gas[12] and liquid chromatographic separations. For this latter application, different methods have been tested to synthesize mesoporous silica particles with spherical shapes and a narrow pore size distribution.[13,14]

Bearing in mind large-scale industrial applications, one has to take into account the critical conditions imposed on molecular sieves. It is recognized that the thermal, hydrothermal, and mechanical stabilities are crucial parameters for potential applications. The powders are usually compressed into pellets and have to withstand extreme reaction and regeneration conditions.

However, M41S materials (MCM-41 and MCM-48) collapse when they are mechanically compressed and have a poor hydrothermal stability in boiling water and steam as a result of silicate hydrolysis of the relative thin amorphous silica walls.[15−18] Because of these limitations, enormous efforts have been made to improve the stability of M41S materials either by changing

* To whom correspondence should be addressed. E-mail: kristof.cassiers@ua.ac.be. Fax: 32-3-820.23.74. Tel.: 32-3-820.23.80.

(1) Kresge, C. T.; Leonowics, M. E.; Roth; W. J.; Vartulli, J. C.; Beck, J. S. *Nature* **1992**, *359*, 710.
(2) Beck, J. S.; Vartuli, J. C.; Roth, W. J.; Leonowics, M. E.; Kresge, C. T.; Schmitt, K. D.; Chu, C. T.-W.; Olson, D. H.; Sheppard, E. W.; McCullen, S. B.; Higgings, J. B.; Schlenker, J. L. *J. Am. Chem. Soc.* **1992**, *114*, 10834.
(3) Tanev, P. T.; Pinnavaia, T. J. *Science* **1995**, *267*, 865.
(4) Tanev, P. T.; Chibwe, M.; Pinnavaia, T. J. *Nature* **1994**, *368*, 321.
(5) Inagaki, S.; Fukushima, Y.; Kuroda, K. *J. Chem. Soc., Chem. Commun.* **1993**, 680.
(6) Galarneau, A.; Barodawalla, A.; Pinnavaia, T. J. *Nature* **1995**, *374*, 529.
(7) Zhao, D.; Feng, J.; Huo, Q.; Melosh, N.; Frederickson, G. H.; Chmelka, B. F.; Stucky, G. D. *Science* **1998**, *279*, 548.
(8) Bagshaw, S. A.; Prouzet, E.; Pinnavaia, T. J. *Science* **1995**, *269*, 1242.
(9) Ryoo, R.; Kim, J. M.; Ko, C. H.; Shin, C. H. *J. Phys. Chem.* **1996**, *100*, 17718.
(10) Baltes, M.; Cassiers, K.; Van Der Voort, P.; Weckhuysen, B. M.; Schoonheydt, R. A.; Vansant, E. F. *J. Catal.* **2001**, *197*, 160.
(11) Corma, A.; Fornés, V.; Navarro, M. T.; Pérez-Patiente, J. *J. Catal.* **1994**, *148*, 569.
(12) Raimondo, M.; Perez, G.; Sinibaldi, M.; De Stefanis A.; Tomlinson, A. A. G. *J. Chem. Soc., Chem. Commun.* **1997**, *15*, 1343.
(13) Grün, M.; Kurganoz, A. A.; Schacht, S.; Schütz, F.; Unger, K. K. *J. Chromatogr. A* **1996**, *740*, 1.
(14) Sierra, L.; Lopez, B.; Guth, J.-L. *Microporous Mesoporous Mater.* **2000**, *39*, 519.
(15) Gusev, V. Y.; Feng, X.; Bu, Z.; Haller, G. L.; O′Brien, J. A. *J. Phys. Chem.* **1996**, *100*, 1985.
(16) Van Der Voort, P.; Baltes, M.; Vansant, E. F. *Catal. Today* **2001**, *68*, 121.
(17) Kawi, S.; Shen, S.-C. *Mater. Lett.* **2000**, *42*, 108.

10.1021/cm0112892 CCC: $22.00
Published on Web 04/09/2002

the synthesis procedure or by modifying the materials after synthesis. For example, the addition of inorganic and organic salts (sodium chlorides, sodium acetates, sodium fluoride, tetraalkylammonium ions, EDTA) during the crystallization process of the pure silica material[18−22] and postsynthesis hydrothermal restructuring in water[23] were reported to enhance the stability in boiling water. Other effective modifications are the complete[24] or partial[25] hydrophobization of the surface by silylation to preclude water attack. The structural stability of silica materials can be improved by increasing the wall thickness and enhancing the local ordering of the amorphous walls.[26] Such thicker-walled and more stable mesoporous silicas were prepared by using a two-step synthetic method or long crystallization times. Other reports have illustrated that incorporated or grafted Al MCM-41 and Al MCM-48 have higher mechanical and hydrothermal stabilities.[17,27,28]

However, as mentioned above, several other synthetic strategies for silica mesostructures have been successfully developed. These materials have slightly different properties than M41S materials, and these differences could lead to an enhancement of the thermal, hydrothermal, and mechanical stabilities. The framework wall thicknesses of HMS and SBA mesostructures are claimed to be consistently larger than those of MCM-41 and MCM-48.[29,30] Alternative synthetic approaches have been reported for the preparation of mesoporous silicate from layered silicates. These materials are designated PCH[6] and FSM[5] and consist of walls that are more condensed and ordered than the walls of M41S materials.

A number of stability studies have already been carried out. The hydrothermal stability in boiling water has been tested on siliceous and Al-grafted MCM-41[17,27] and pure MCM-48.[18] Furthermore, the steam resistances of pure, Al-grafted,[27] and Al-incorporated[28] MCM-41 and pure and V-grafted methylsilylated MCM-48[25] have been investigated. In addition, O'Brien et al.[15] and Hartmann et al.[31] focused on the mechanical stabilities of both MCM-41 and MCM-48, whereas the thermal stabilities of MCM-41 and FSM were tested by Inagaki et al.[32] However, the various stability tests summarized above were performed under different conditions. This variation in experimental parameters makes it difficult to make a systematic comparison between the different tests on one hand and the several silica materials on the other. In addition, the reported stability experiments were performed only on M41S materials. So far, there have been no reports on any systematic comparison of thermal, hydrothermal, and mechanical stabilities among the different recently developed mesoporous silica materials.

This current work presents the first systematic and comparative study of the thermal, hydrothermal, and mechanical stabilities of the most important mesoporous materials, in particular, the molecular sieves MCM-41, MCM-48, HMS, FSM-16, PCH, and SBA-15, and it can be considered as a basis for further investigations of the stability of mesoporous materials.

Experimental Section

Syntheses. M41S materials synthesized with TEOS [denoted MCM-41(T) and MCM-48(T)] and fumed silica [denoted MCM-41(FS) and MCM-48(FS)] as the silica precursor, respectively, HMS, FSM-16, PCH, KIT-1, and SBA-15 were prepared according to syntheses reported in the literature.[5,7,9,23,29,33−35] For all of these materials, recently published high-quality syntheses were selected.

MCM-41. A gel mixture with the composition SiO_2/TEAOH/CTMABr/H_2O = 1/0.2/0.25/35 was used. Water and CTMABr were stirred at room temperature. Additionally, the TEAOH solution and the silica source were added. After being stirred for 2 h at 70 °C, the mixture was aged for 24 h at room temperature. Then, it was transferred into an autoclave at 150 °C for 48 h. The filtration cake was then washed with water and again put in an autoclave with water for 72 h at 150 °C.

KIT-1. KIT-1 was prepared with colloidal silica as the silica source and CTABr as the surfactant with a gel composition of SiO_2/Na_2O/CTABr/$(NH_4)_2O/Na_4EDTA/H_2O$ = 4/1/1/0.15/8/300. The synthesis procedure is similar to that used for MCM-41 and is further described in ref 9.

HMS. HMS was synthesized at room temperature using dodecylamine (DDA) as the structure-directing agent and tetraethyl orthosilicate (TEOS) as the silica source with molar ratios of TEOS/DDA/ethanol/H_2O = 1/0.27/9.09/29.6. DDA was first dissolved in ethanol. To this mixture, water and then TEOS were added. After the mixture was stirred for 18 h, the resulting white solid was filtered and air-dried.

MCM-48. MCM-48 materials were prepared using the gemini 16−12−16 cationic surfactant with the general formula $[C_nH_{2n+1}-N^+(CH_3)_2-(CH_2)_s-N^+-(CH_3)_2C_mH_{2m+1}]2Br^-$ with molar gel compositions of surfactant/NaOH/H_2O/TEOS = 0.06/0.6/150/1 and surfactant/NaOH/H_2O/SiO_2 = 0.1/0.26/100/1 for MCM-48(T) and MCM-48(FS), respectively. Both syntheses are similar to the preparation of MCM-41 and are described in refs 33 and 35.

FSM-16. FSM-16 was prepared with CTMABr as the template and kanemite ($NaHSi_2O_5 \cdot 3H_2O$) as the silica source. Kanemite was synthesized according to a procedure reported elsewhere.[36] Ten grams of kanemite was dispersed in 200 mL of a 0.1 M solution of CTMABr, and the mixture was heated at 70 °C for 3 h with stirring. The pH of the suspension was kept at 8.5 for a further 3 h by the addition of 2 M HCl with stirring.

PCH. PCH was synthesized with synthetic saponite and TEOS as the silica source. CTMABr (Q^+Br^-) acts as a surfactant in cooperation with DDA at a molar ratio of Q^+-saponite/DDA/TEOS = 1/4/30. Saponite (2 g) was mixed with a solution

(18) Jun, S.; Kim, J. M.; Ryoo, R.; Ahn, Y.-S.; Han, M.-K. *Microporous Mesoporous Mater.* **2000**, *41*, 119.
(19) Ryoo, R.; Jun, S. *J. Phys. Chem. B* **1997**, *101*, 317.
(20) Kim, J. M.; Jun, S.; Ryoo, R. *J. Phys. Chem. B* **1999**, *103*, 6200.
(21) Das, D.; Tsai, C.-M.; Ceng, S. *J. Chem. Soc., Chem. Commun.* **1999**, 473.
(22) Xia, Q.-H.; Hidajat, K.; Kawi, S. *Mater. Lett.* **2000**, *42*, 102.
(23) Chen, L.; Horiuchi, T.; Mori, T.; Maeda, K. *J. Phys. Chem. B* **1999**, *103*, 1216.
(24) Koyano K. A.; Tatsumi T.; Tanaka Y.; Nakata S. *J. Phys. Chem. B* **1997**, *101*, 9436.
(25) Van Der Voort, P.; Baltes, M.; Vansant, E. F. *J. Phys. Chem. B* **1999**, *103*, 10102.
(26) Mokaya, R. *J. Phys. Chem. B* **1999**, *103*, 10204.
(27) Mokaya, R.; Jones, W. *J. Chem. Soc., Chem. Commun.* **1998**, 1839.
(28) Shen, S.-C.; Kawi, S. *J. Phys. Chem. B* **1999**, *103*, 8870.
(29) Tanev, P. T.; Pinnavaia T. J. *Chem. Mater.* **1996**, *8*, 2068.
(30) Kruk, M.; Jaroniec, M.; Ko, C. H.; Ryoo, R. *Chem. Mater.* **2000**, *12*, 1961.
(31) Hartmann, M.; Bischof, C. *J. Phys. Chem. B* **1999**, *103*, 6230.
(32) Inaki, Y.; Yoshida, H.; Kimura, K.; Inagaki, S.; Fukushima, Y.; Hattori T. *Phys. Chem. Chem. Phys.* **2000**, *2*, 5293.
(33) Van Der Voort, P.; Mathieu, M.; Mees, F.; Vansant, E. F. *J. Phys. Chem. B* **1998**, *102*, 8847.
(34) Ahenach, J.; Cool, P.; Vansant, E. F. *Phys. Chem. Chem. Phys.* **2000**, *2*, 5750.
(35) Collart, O.; Van Der Voort, P.; Vansant, E. F.; Desplantier-Gescard, D.; Galarneau, A.; Di Renzo, F.; Fajula, F. *J. Phys. Chem. B* **2001**, *105*, 12771.
(36) Beneke, K.; Lagaly, G. *Am. Mineral.* **1977**, *62*, 763.

Table 1. Effect of Thermal and Hydrothermal Treatments on the Surface Area and Primary Pore Volume of Mesoporous Materials

treatment conditions	MCM-48(T)	MCM-48(FS)	MCM-41(T)	MCM-41(FS)	KIT-1	FSM-16	HMS	SBA-15	PCH
				surface area					
550 °C	1433	1319	1128	1027	1059	1172	1021	632	899
650 °C	1248	1321	1114	970	1078	1112	957	561	881
750 °C	108	1287	403	879	983	915	213	446	739
850 °C	*a*	1094	*a*	795	967	476	*a*	*a*	441
400 °C, 30 vol % steam, 48 h	1357	1176	1048	892	*a*	995	915	533	838
400 °C, 30 vol % steam, 120 h	1318	1130	1019	864	*a*	789	830	500	728
100 °C, 100% relative humidity, 16 h	197	168	145	106	974	67	228	281	335
				primary pore volume					
550 °C	1.14	1.22	0.95	0.92	0.88	0.78	0.81	0.63	0.50
650 °C	0.73	1.13	0.87	0.76	0.87	0.63	0.58	0.56	0.49
750 °C	*b*	0.94	0.26	0.68	0.76	0.44	*b*	0.48	0.41
850 °C	*a*	0.74	*a*	0.53	0.68	0.20	*a*	*a*	0.25
400 °C, 30 vol % steam, 48 h	1.00	1.00	0.72	0.66	*a*	0.52	0.57	0.57	0.49
400 °C, 30 vol % steam, 120 h	0.93	0.94	0.47	0.58	*a*	0.36	0.48	0.55	0.43
100 °C, 100% relative humidity, 16 h	*b*	*b*	*b*	*b*	0.78	*b*	*b*	0.47	*b*

[a] Not measured. [b] No capillary condensation step was observed in the N_2 isotherm.

of 0.1 M CTMABr for 24 h at 50 °C. Subsequently, the reaction of Q^+-saponite with DDA was performed for 30 min and with TEOS for 4 h.

SBA-15. SBA-15 was synthesized using Pluronic 123 triblock copolymer ($EO_{20}-PO_{70}-EO_{20}$) as the template and TEOS as the silica precursor. Pluronic 123 (4 g) was dissolved in 30 mL of water and 120 mL of a 2 M HCl solution. Then, 10.7 mL of TEOS was added, and the resulting mixture was aged for 20 h at 35 °C and for 24 h at 80 °C.

Characterization of Materials. X-ray diffractograms were recorded on a Philips PW1840 powder diffractometer, using Ni-filtered Cu Kα radiation. Porosity and surface area studies were performed with a Quantachrome Autosorb-1-MP automated gas adsorption system. All samples were outgassed for 16 h at 200 °C prior to adsorption. Gas adsorption was performed using nitrogen as the adsorbate at liquid nitrogen temperature (77 K).

Thermal Stability. To assess thermal stability, all samples were calcined in air starting from an end temperature of 550 °C. The end temperature was increased in steps of 100 °C as long as no complete collapse of the mesostructure occurred. All of the sample precursors were calcined at a heating rate of 2 °C/min and kept at the end temperature for 8 h.

Hydrothermal Stability. The hydrothermal stability study was conducted by exposing the samples to a N_2 stream containing 30 vol % of water vapor at 400 °C for 48 and 120 h. The flow of the N_2 stream was kept at 100 mL/min with a pressure of 1 atm. In addition, all samples were also exposed to steam in a more severe test at 100 °C for 16 h at autogenous pressure with a relative humidity of 100%.

Mechanical Stability. Mechanical tests were performed by pelletizing each powder into a die with a diameter of 13 mm. The pressure was increased in steps of 74 MPa and was kept constant for 2 min.

Calculation Methods. Surface areas were calculated according to the BET equation[37] using adsorption data in a relative range from 0.05 to 0.3. Mesopore size distributions were calculated from the adsorption isotherm using the BJH method. Primary mesopore volumes (V_p) were measured after the capillary condensation step. To evaluate the wall thickness, a reliable value of mesopore size is required. To calculate this mesopore size, it is generally agreed that the maximum of the BJH method underestimates the sizes of pores.[38,39] Therefore, the more precise geometrical relation $D_{geom} = cd(\rho V_p)^{1/2}/(1 + \rho V_p)^{1/2}$, developed for hexagonal mesostructures,[40] was used to calculate the primary mesopore diameters of MCM-41, FSM-16, HMS, and SBA-15. In the formula, $c = 1.213$, $\rho = 1.6$ g/cm^3 and represents the density of silica in the walls,[41] d represents the lattice spacing of d_{100}, and V_p is the primary mesopore volume. The wall thickness, b_{hexag}, for hexagonal materials was evaluated using the relation $b_{hexag} = a - 0.95D_{geom}$, where a represents the unit cell parameter and 0.95 is the factor required to take into account the hexagonal section of the pore. This geometrical model cannot be applied to the cubic MCM-48. However, the wall thickness of MCM-48 was calculated from adsorption and XRD data using a theory developed recently by Neumark et al., resulting in the easily applicable formula $b_{cubic} = a/3.0919 - D_{cubic}/2$.[42] D_{cubic} was obtained from the maximum of the Kruk−Jaroniec−Sayari (KJS) pore size distribution, which is based on a corrected Kelvin equation and is reported to render a much more accurate value than the BJH maximum for MCM-48 materials.[43,44]

Results and Discussion

Thermal Stability. Table 1 shows the surface area and primary mesopore volume calculated from N_2-sorption measurements for all of the thermally and hydrothermally treated samples. After calcination at 550 °C for 8 h, all of these mesoporous materials have essentially the same structural and physical properties as described in their original reports. MCM-41 prepared with TEOS and fumed silica, FSM-16, SBA-15, HMS, and KIT exhibit well-defined 100 reflections in their XRD patterns, which are characteristic for hexagonal mesostructures. Moreover, MCM-41(T), MCM-41(FS),

(37) Sing, K. S. W.; Everett, D. H.; Haul, R. A. W.; Moscou, L.; Pierotti, R. A.; Rouquerol, J.; Siemieniewska, T. *Pure Appl. Chem.* **1985**, *57*, 603.

(38) Galarneau A.; Desplantier, D.; Dutartre, R.; Di Renzo, F. *Microporous Mesoporous Mater.* **1999**, *27*, 297.

(39) Zhu, H. Y.; Zhao, X. S.; Lu, G. Q. Do, D. D. *Langmuir* **1996**, *12*, 6513.

(40) Kruk, M.; Jaroniec, M.; Sayari, A. *Chem. Mater.* **1999**, *11*, 492.

(41) Kim, J. M.; Ryoo, *R. Bull. Korean Chem. Soc.* **1996**, *17*, 66.

(42) Ravikovitch, P. I.; Neumark, A. V. *Langmuir* **2000**, *16*, 2419.

(43) Kruk, M.; Jaroniec, M.; Sayari, A. *Langmuir* **1997**, *13*, 6267.

(44) Kruk, M.; Jaroniec, M.; Ryoo, R.; Joo, S. H. *Chem. Mater.* **2000**, *13*, 1414.

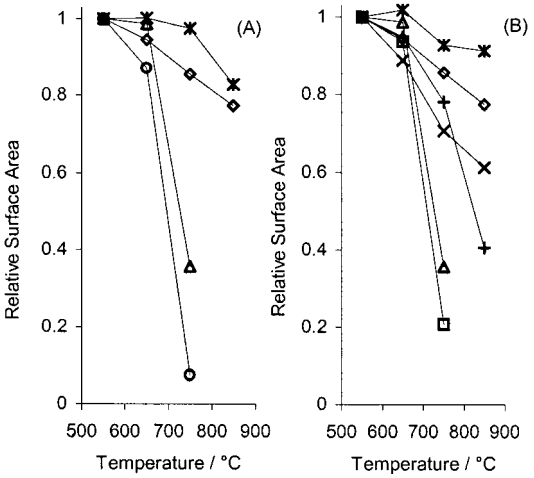

Figure 1. Relative surface area as a function of temperature for (A) the M41S materials MCM-41(T) (△), MCM-48(T) (○), MCM-41(FS) (◇), and MCM-48(FS) (*) and (B) the hexagonally ordered materials HMS (□), MCM-41(T) (△), FSM-16 (+), SBA-15 (×), MCM-41(FS) (◇), and KIT-1 (*).

FSM-16, and SBA-15 have additional relatively narrow 110 and 200 diffraction lines in their XRD patterns, indicating greater long-range order than in HMS, which has only a broad 100 reflection line. Furthermore, the MCM-48 materials prepared with TEOS and fumed silica, denoted by MCM-48(T) and MCM-48(FS), respectively, also show very high degrees of pore ordering, with two intense reflections in the region $2\theta = 1-4°$, assigned to the 211 and 220 reflections, which are both characteristic for the cubic *Ia*3*d* space group. Finally, PCH shows a broad 100 reflection related to the parallel ordering of the clay sheets.

It can be seen from Table 1 that the surface areas and primary mesopore volumes of all tested mesoporous materials gradually decrease as the calcination temperature increases. The relative decrease in surface area is presented in Figure 1a and b for M41S materials and hexagonal mesostructures, respectively. To gain insight in the influence of the temperature on the porous networks, Figure 2 displays the isotherms of MCM-48-(T), MCM-48(FS), FSM-16, and SBA-15 as a function of calcination temperature.

M41S Materials. A close inspection of the surface area data clearly indicates that MCM-41(T) and MCM-48-(T) show similar thermal behaviors. It is interesting to note the superior heat resistance of M41S materials prepared with fumed silica compared to the TEOS-made MCM-41(T) and MCM-48(T). When subjected to a calcination temperature of 750 °C, these TEOS-made materials suffer an ~80% decrease in BET surface area, whereas, in the case of M41S materials prepared with fumed silica, around 80% of the initial surface area still remains after calcination at 850 °C. Furthermore, as can be seen in Figure 2, the pore structure of MCM-48-(T) is already completely degraded at 750 °C, as reflected in the disappearance of the capillary condensation step in the N_2 isotherm and the diffraction lines of the XRD pattern (not shown). A very similar trend can be observed for the MCM-41(T) mesostructure. In addition, it is very interesting to observe that the shapes of the isotherms for MCM-41(FS) and MCM-48(FS) remain almost unchanged even when these materials have been subjected to a calcination temperature of 850

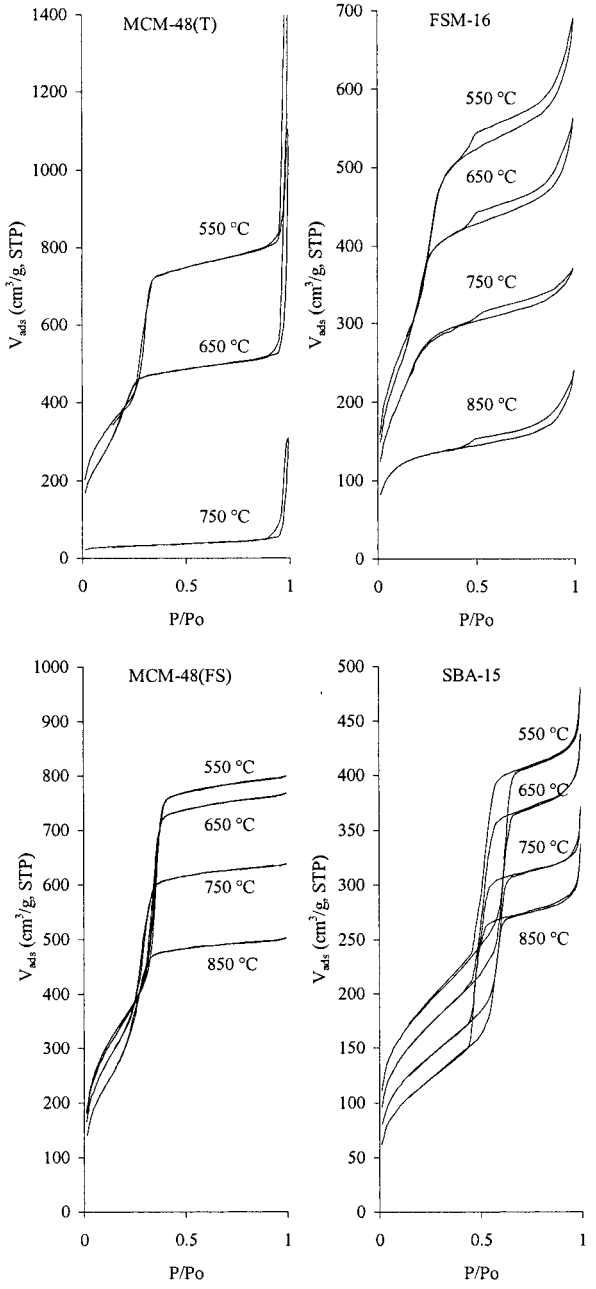

Figure 2. N_2 adsorption−desorption isotherms as a function of calcination temperature for MCM-48(T), MCM-48(FS), FSM-16, and SBA-15.

°C. A sharp inflection in the isotherm [see also Figure 2 for MCM-48(FS)] and clear and sharp characteristic diffraction lines can still be found at this temperature. Moreover, unit cell contraction is almost negligible when the calcination temperature is increased from 550 to 850 °C [from 47.8 to 43.4 Å for MCM-41(FS) and from 88.9 to 84.8 Å for MCM-48(FS)]. However, the synthesis conditions are exactly the same for the M41S materials prepared with TEOS and the corresponding M41S mesostructures prepared with fumed silica. In this study, MCM-48 and MCM-41 mesostructures were formed by the electrostatic assembly of cationic 16−12−16 gemini surfactants and cationic quaternary ammonium surfactants, respectively, both in interaction with anionic silica species under hydrothermal conditions. For both types of M41S material, exactly the same temperatures and treatment times were applied, so that

Table 2. Lattice Parameters *a*, Geometric and KJS Pore Diameters, and Wall Thicknesses for Hexagonal and Cubic Mesostructures

sample	a (Å)	D_{geom} (Å)	D_{KJS} (Å)	b_{hexag} (Å)	b_{cubic} (Å)
MCM-41(T)	43.0	35.1	–	9.7	–
MCM-41(FS)	47.8	38.7	–	11.0	–
KIT-1	45.1	36.2	–	10.7	–
FSM-16	38.5	30.1	–	9.9	–
HMS	42.7	33.7	–	10.7	–
SBA-15	95.2	68.9	–	29.7	–
MCM-48 (T)	83.1	–	35.1	–	9.3
MCM-48 (FS)	89.1	–	38.8	–	9.4

the only major difference between the TEOS and fumed silica samples is the silica precursor. Furthermore, despite the remarkable difference in heat resistance between corresponding M41S materials prepared with TEOS and fumed silica, these materials show no significant mutual differences in wall thickness, as can be inferred from Table 2. It should also be mentioned that the synthesis of MCM-48 with TEOS already results in a material with a somewhat lower quality. This can be seen in the steep increase in the adsorption volume at $P/P_0 = 0.9-1$ in Figure 2 (high interparticular porosity). These results imply a strong correlation between the silica source used in the synthesis of M41S materials and the structural degradation occurring upon thermal treatment.

Other Mesostructures. As seen in Figure 1b, HMS shows a thermal stability similar to that of MCM-41(T) and MCM-48(T). At a calcination temperature of 750 °C, no structural mesoporosity can be detected, and the surface area is reduced to around 20% of its initial value. Furthermore, the clay-based materials FSM-16 and PCH also show a similar trend but the relative drop in surface area is smaller than it is for HMS, MCM-41(T), and MCM-48(T). At 850 °C, around 50% of the initial surface area still remains. Figure 2 provides further evidence that the thermal stability of FSM-16 is higher than that of MCM-48(T). There is still a small capillary condensation step in the isotherm and a 100 reflection in the XRD diffractogram at a calcination temperature of 750 °C, but both disappear at 850 °C as a result of the complete collapse of the framework confined mesopores. A parallel trend can be observed for PCH, the other clay-based material. Furthermore, SBA-15 and KIT-1 show a heat resistances that are very similar to those of M41S materials prepared with fumed silica. At a calcination temperature of 850 °C, only a small shrinkage of the BJH diameter (from 29.7 to 26.8 Å for KIT-1 and from 55.7 to 48.7 Å for SBA-15) and a slight diminution of pore volume (see Table 1) can be observed.

To make a clear comparison between the studied hexagonal mesostructures [MCM-41(T), MCM-41(FS), KIT-1, HMS, FSM-16, and SBA-15], accurate calculations of the wall thickness were performed (Table 2). FSM-16, MCM-41(T), MCM-41(FS), KIT-1, and HMS show no significant differences in wall thickness (10.4 ± 0.7 Å). HMS is prepared with TEOS, and it is therefore not surprising that this material exhibits a heat resistance similar to that of the TEOS-made MCM-41(T). Furthermore, the higher thermal stability of FSM-16 compared to hexagonal TEOS-made materials with the same wall thickness can be attributed to the higher regular arrangement in the silica walls.[32] Additionally, SBA-15, which is also prepared with TEOS, shows a much higher thermal stability than the other tested hexagonal TEOS-made mesostructures. One should note that the wall thickness of SBA-15 is almost 3 times larger (29.7 Å) than those of HMS (10.7 Å) and MCM-41(T) (9.7 Å). Therefore, one can infer that the wall thickness also has a decisive influence on the thermal stability.

Hydrothermal Stability. The hydrothermal stabilities of template-free mesostructures were studied by treating the samples with steam at high temperature. To make a clear and systematic comparison of hydrothermal stabilities of the different investigated materials, a relatively mild steaming test was performed that did not completely "destroy" the mesostructures but showed clear differences in the resulting physical characteristics. On the other hand, a severe test was carried out to indicate which materials could withstand extreme steaming conditions. The physical properties for the different mesoporous materials before (samples calcined at 550 °C) and after the various hydrothermal treatments are also listed in Table 1. Furthermore, the changes in the pore size distribution (based on the BJH method) as a result of the mild steaming treatments at 400 °C are shown in Figure 3 for all tested materials. For SBA-15, MCM-48(T), MCM-48(FS), and PCH, a clear retention of the initial structural uniformity can be observed, even after a treatment of 120 h. This is further confirmed by the observation that they all show only a small relative decrease in primary mesopore volume (15−20% of the initial mesopore volume). In contrast, a significant loss of pore structure can be observed for HMS, MCM-41(T), MCM-41(FS), and FSM-16, even already after a treatment of 48 h. This deformation gradually increases with longer treatment time. In addition to a broadening of the pore size distribution, a decrease in pore size can also be observed for these materials. Moreover, as listed in Table 3 and shown in Figure 4, the loss in structural ordering is also reflected in a ∼40% decrease of mesopore volume for HMS and MCM-41(FS) and even a ∼50% decrease for FSM-16 and MCM-41(T) after a treatment of 120 h. These results indicate that the deformation of the examined samples does not follow the same trend as in the case of the thermal treatment. Next to a similar hexagonal ordering and a comparable and beneficial decrease in pore structure after hydrothermal treatment, HMS, MCM-41(T), MCM-41(FS), and FSM-16 all display almost the same wall thickness, as can be inferred from Table 2. However, these materials are synthesized with a variety of silica sources. This suggests that, in contrast to the trend observed in the thermal stability test, the silica source does not play a significant role in the hydrothermal stability. Furthermore, it can be additionally emphasized that, with the exception of the silica precursor, MCM-41(T) and MCM-41(FS) are very similar materials with the same wall thickness prepared under exactly the same conditions, whereas no remarkable differences in hydrothermal stability can be observed. Moreover, one should note the difference in hydrothermal stability between HMS and MCM-41(T) on one hand and SBA-15 on the other hand. Despite the fact that these materials are synthesized with the same silica source (TEOS), SBA-15 is hydrothermally much more stable than HMS and MCM-41-

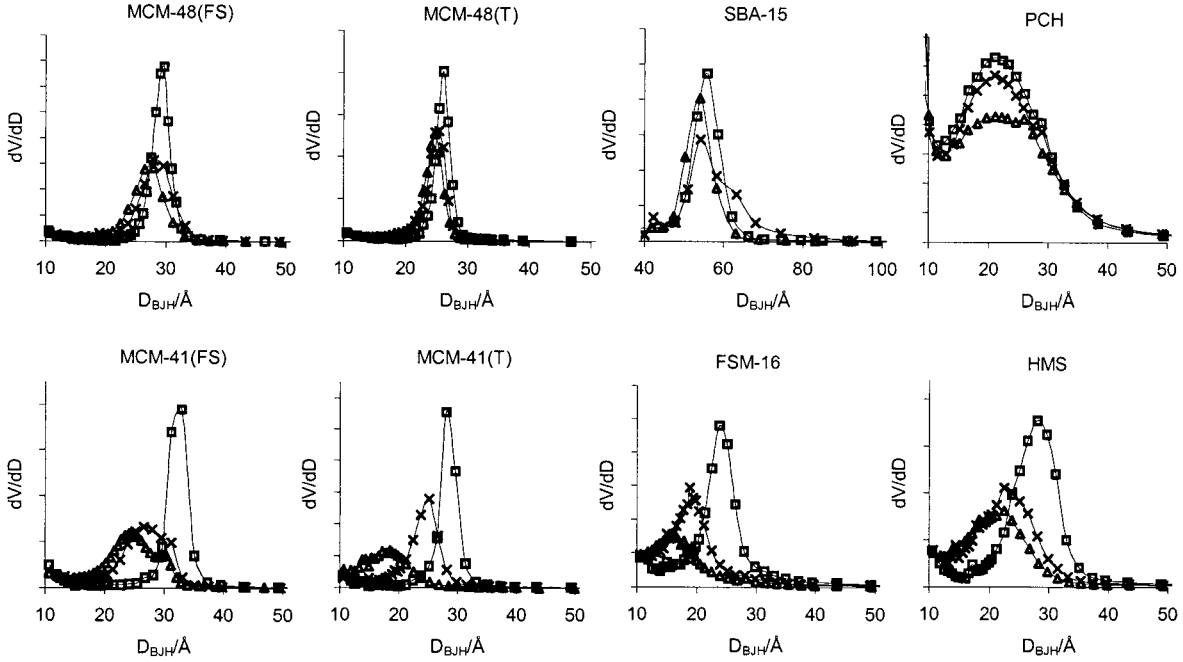

Figure 3. BJH pore size distributions for all samples before (□) and after mild hydrothermal treatment at 400 °C for 2 (×) and 5 days (△).

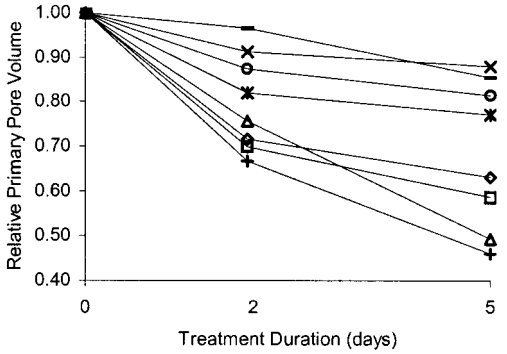

Figure 4. Relative primary pore volume as a function of mild hydrothermal treatment time for FSM-16 (+), MCM-41(T) (△), HMS (□), MCM-41(FS) (◇), MCM-48(FS) (*), MCM-48(T) (○), PCH (−), and SBA-15 (×).

Table 3. BJH Pore Diameter and Relative Decrease of BJH Pore Diameter after Mild Hydrothermal Treatment

sample	BJH pore diameter (Å) 0 h	48 h	120 h	relative decrease after 120 h (%)
MCM-41(T)	28.0	25.2	18.5	33.9
MCM-41(FS)	31.7	26.6	24.7	22.1
FSM-16	23.8	18.9	16.6	30.3
HMS	28.1	26.6	22.5	20.0
MCM-48(T)	26.1	25.4	25.4	2.7
MCM-48(FS)	29.7	28.0	28.0	5.8
SBA-15	55.7	54.0	53.9	3.2
PCH	22.3	22.3	22.2	0.0

(T). It is reasonable to suggest that this higher hydrothermal stability of SBA-15 is a result of the thicker pore walls (Table 2) and is in agreement with the results reported in other papers.[26] It is believed that the structural degradation is caused by the hydrolysis of Si−O−Si bonds.[45] If the walls are thin, as in the case of HMS, FSM-16, MCM-41(T), and MCM-41(FS) (thicknesses of ∼10 Å, which corresponds to only a few $[SiO_4]^{4-}$ groups), these structures collapse easily by hydrolysis. A possible explanation for the low structural damage of MCM-48 under mild steaming conditions can be found in the fact that MCM-48 has a different pore structure and curvature, which results in a different nature of surface silanol groups.[46] Therefore, MCM-48 has a higher hydrophobicity than MCM-41, resulting in a higher steam resistance.

Furthermore, it is difficult to compare PCH with the other tested materials because it has a completely different and more complex pore structure that does not allow for the wall thickness to be calculated. However, it appears that PCH exhibits a hydrothermal stability under mild treatment conditions similar to those of SBA-15, MCM-48(T), and MCM-48(FS).

To indicate which material has the highest hydrothermal stability, all of the materials were subjected to a severe steaming test by exposing the samples to steam at autogenous pressure. The physical characteristics are also summarized in Table 1, and Figure 5 presents the isotherms of the steamed KIT-1, SBA-15, and MCM-48(T) samples after 16 h. It can be inferred from this figure that only KIT-1 and SBA-15 can withstand this test. Despite the significant loss of BET surface area for SBA-15, a clear capillary condensation step can still be observed, whereas no porosity is present for MCM-48(T). Similarly, the same structural collapse as was observed for MCM-48(T) was obtained for MCM-48(FS), MCM-41(T), MCM-41(FS), HMS, FSM-16, and PCH, with the BET surfaces being reduced to 100−300 m^2/g. These findings clearly confirm that the wall thickness has a great influence on the hydrothermal stability. Although the KIT-1 material has a wall thickness similar to that of the collapsed materials, it can withstand this steaming test with only a very small decrease in physical properties. An explanation for this behavior

(45) Tatsumi, T.; Koyano, K. A.; Tanaka, Y.; Nakata, S. *Chem. Lett.* **1997**, *5*, 469.

(46) Landmesser, H.; Kosslick, H.; Storek, W.; Fricke, R. *Solid State Ionics* **1997**, 101−103, 271.

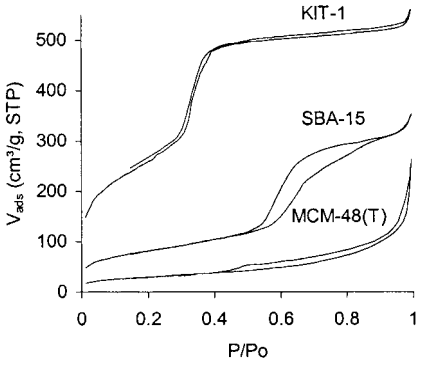

Figure 5. N_2 adsorption−desorption isotherms of KIT-1, SBA-15, and MCM-48(T) after severe hydrothermal treatment at autogenous pressure.

can be found in the condensation degree of the silica walls of the KIT-1 material. Chen et al.[23] reported that the degree of polymerization in the silica walls plays a crucial role in the hydrothermal stability by comparing a postsynthetically restructured MCM-41 with a non-restructured MCM-41. KIT-1 was prepared in the presence of EDTA salt, and it is known from earlier reports that the addition of EDTA or other salts[18−22,47] remarkably improves the degree of silicate polymerization in the silica walls. Therefore, KIT-1 displays a remarkable hydrothermal stability.

Mechanical Stability. X-ray diffraction patterns of the compressed samples were recorded up to a pressure at which the intensities of the diffraction peaks were reduced to 10% of their initial values. For samples pelletized at a pressure of 296 MPa, N_2 sorption isotherms were recorded to evaluate the structural degradation. In all cases, the intensities of the X-ray diffraction lines decreased markedly with increasing pelletizing pressure, as shown for MCM-41(FS) in Figure 6. Simultaneously, the steep increase in the N_2 adsorption isotherms due to the filling of mesopores is less pronounced, and the amount of adsorbed N_2 is reduced after the application of external pressure. Table 4 summarizes the effects of unilateral compression on the lattice parameter *a*, the primary pore volume, the BJH pore diameter, and the specific BET surface area and represents the pelletizing pressure at which only 10% of the initial X-ray diffraction intensity remains. The ordered mesoporosity is essentially lost for all mesostructures at pelletizing pressures of 370 ± 74 MPa, as indicated by the absence of the steep adsorption step in the N_2 isotherm and the disappearance of the peaks in the X-ray diffraction pattern [Figure 6 for MCM-41(FS)]. This order of magnitude is similar to those reported previously for MCM-41, MCM-48, and FSM-16.[31,45,48,49] It should be noted that only small differences in mechanical stability between the different materials could be seen. At a compression of 296 MPa, the N_2 adsorption data show that FSM-16 and MCM-48(T) are more fragile than the other samples. The BET surface area in both cases is reduced to 45% of its initial

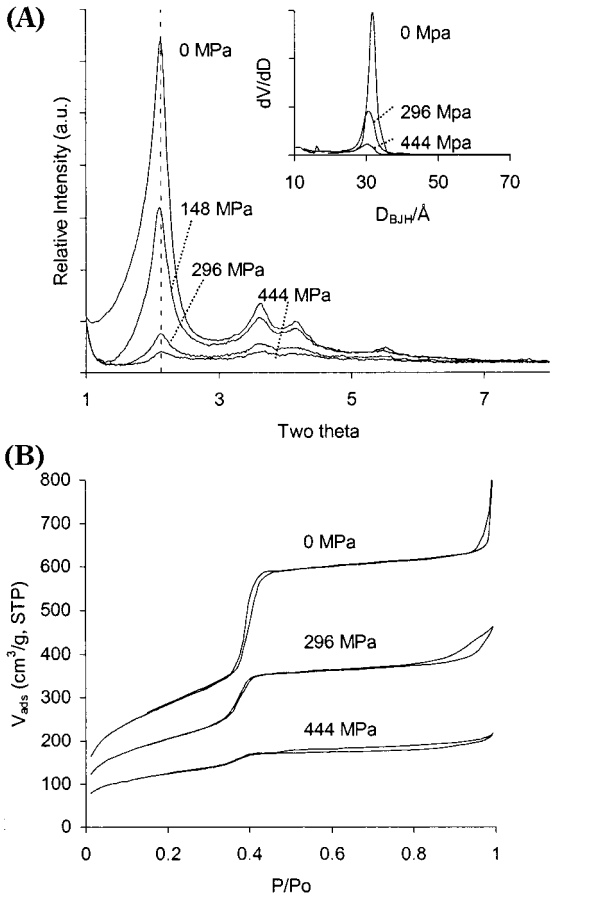

Figure 6. (A) X-ray diffractograms and (B) N_2 adsorption−desorption isotherms of MCM-41(FS) pelletized with pressures between 0 and 444 MPa. The inset in Figure 6A represents the BJH pore size distributions of parent and compressed MCM-41(FS) samples.

Table 4. Physical Properties before and after Mechanical Pressure of 296 MPa

sample	pressure (MPa)	*a* (Å)	BJH PD[a] (Å)	PV[b] ($cm^3\ g^{-1}$)	BET SA[c] ($m^2\ g^{-1}$)	max pressure (MPa)
MCM-41(T)	0	43.0	28.0	0.95	1128	370
	296	43.0	28.0	0.65	856	
MCM-41(FS)	0	47.8	31.7	0.92	1027	444
	296	47.2	31.1	0.54	729	
MCM-48(T)	0	83.1	26.1	1.14	1433	296
	296	81.6	25.3	0.35	657	
MCM-48(FS)	0	89.1	29.7	1.22	1319	370
	296	88.9	28.4	0.73	932	
KIT-1	0	45.1	29.7	0.88	1059	444
	296	45.9	29.4	0.67	911	
FSM-16	0	38.5	23.8	0.78	1172	296
	296	38.5	−	−	532	
HMS	0	42.7	28.1	0.81	1021	370
	296	36.5	23.9	0.39	812	
SBA-15	0	95.2	55.7	0.63	632	444
	296	94.0	53.3	0.48	573	

[a] BJH pore diameter [b] Pore volume. [c] BET surface area.

value, whereas only a 10−30% decrease was found for the other materials at this stage of compression. Similarly, a much higher pore volume decrement can be seen for FSM-16 and MCM-48(T). It should be emphasized that no clear trends can be observed. However, it appears that M41S materials synthesized with fumed silica have somewhat higher mechanical stabilities than those prepared with TEOS. Furthermore, SBA-15 and KIT-1 show the smallest decrease of mesopore volume (25%) and surface area (10%) after compression at 296

(47) Yu, J.; Shi J.-L.; Chen, H.-R.; Yan, J.-N.; Yan, D.-S. *Microporous Mesoporous Mater.* **2001**, *46*, 153.
(48) Springuel-Huet, M.-A.; Bonardet J.-L.; Gédéon, A.; Yue, Y.; Romannikov, V. N.; Fraissard, J. *Microporous Mesoporous Mater.* **2001**, *44*−*45*, 775.
(49) Ishikawa, T.; Matsuda, M.; Yasukawa, A.; Kandori, K.; Fukushima, T.; Kondo, S. *J. Chem. Soc., Faraday Trans.* **1996**, *92*, 1985.

MPa. An explanation for this notable feature can be found in the nature of the mechanism of collapse. As shown previously, the structural decay is a consequence of the cleavage of Si−O−Si by adsorbed water promoted by compression.[45,49] MCM-41(T), MCM-41(FS), MCM-48(T), MCM-48(FS), HMS, and FSM-16 all have wall thicknesses of around 10 Å (see Table 2), which corresponds to only 3 $[SiO_4]^{4-}$ layers, whereas SBA-15 has a wall thickness of 29.7 Å, corresponding to around 10 $[SiO_4]^{4-}$ layers. Furthermore, as mentioned above, KIT-1 has very condensed silica walls. Consequently, it is not surprising that the much thicker pore walls of SBA-15 and the highly polymerized walls are less affected by this systematic mechanochemical cleavage process. Nevertheless, it should be emphasized that both SBA-15 and KIT-1 show no resulting X-ray diffraction lines at a pelletizing pressure of 444 MPa despite the inferior sensitivity to mechanical pressure at 296 MPa. The large porosity and the absence of a stabilizing crystal structure can explain the relatively slight differences in the final mechanical stabilities of all studied materials. Therefore, these materials show inferior mechanical stabilities compared to zeolites.[50,51]

A more detailed examination of the physical data permits a closer look at the influence of unilateral pressure on the structural properties of the mesoporous materials. As can be seen in Table 4, except for HMS, the specific surface area and mesopore volume are reduced in all cases, whereas the BJH pore diameter and the cell parameter are unaffected. Furthermore, the pore size distributions for these materials are only slightly broadened, as shown in Figure 6 for MCM-41-(FS), which indicates only minimal pore deformation upon compression. This indicates either that some of the pores are blocked by other particles of the same material or that less stable pores are completely collapsed due to compression while the residual pores are totally unaffected. In contrast, HMS exhibits a smaller BJH maximum and unit cell parameter after pelletization at 296 MPa, while its pore size distribution is merely slightly broadened. Contrary to all of the other studied materials, one can therefore suggest that the lattice of HMS has a certain flexibility.

Conclusion

The thermal stability is found to be strongly related to the wall thickness and the silica precursor used during synthesis. It is shown that M41S materials prepared with fumed silica are thermally stable to at least 850 °C, whereas materials prepared with TEOS are completely collapsed at a calcination temperature of 750 °C. Nevertheless, the TEOS-made materials have exactly the same wall thickness and are prepared under the same hydrothermal conditions as the corresponding fumed-silica-made materials. By comparing hexagonal mesostructures with similar wall thicknesses, the following stability trend can be observed: KIT-1 (colloid silica), MCM-41 (fumed silica) > FSM16 (layered silicate) > MCM-41 (TEOS), HMS (TEOS). Although SBA-15 is also prepared with TEOS, it shows a much higher thermal stability than HMS and MCM-41 synthesized with TEOS. This can be explained by its 3-times-thicker pore walls.

It was observed that the structural deformation of the examined samples does not follow the same trend after a mild hydrothermal treatment at 400 °C with 25% steam at 1 atm pressure as it does after thermal treatment. It was observed that the hydrothermal stability is influenced by three factors. First, materials with very polymerized or thicker pore walls are less affected under these steaming conditions. SBA-15 and KIT-1 can therefore even withstand a more severe test under autogenous pressure, whereas the other molecular sieves are completely destroyed. Under mild steaming conditions, a third factor becomes more important for all materials with comparable wall thicknesses. It was observed that the structural degradation of cubic MCM-48 is lower than that of the hexagonal mesoporous materials HMS, MCM-41, and FSM-16, which might be a result of its different pore structure and curvature, resulting in a lower affinity toward water for MCM-48.

No remarkable trends can be observed for the mechanical stability. The mesoporosity is essentially lost for all mesostructures at pelletizing pressures of around 444 MPa. Nevertheless, these ordered mesoporous structures show mechanical stabilities that are inferior to those of zeolites, which might result from their large porosity and the absence of a stabilizing crystal structure.

Finally, it should be mentioned that, despite the interesting features of SBA-15 and KIT-1, none of the materials reported in this paper exhibit superior stability behavior for all tests. Therefore, much work still remains to be done to stabilize existing or develop new mesoporous materials, and the evaluation of the stabilities of these mesostructures should be taken with care.

Acknowledgment. P.V.D.V. and P.C. thank the FWO (Fund for Scientific Researsch, Flanders, Belgium) for senior research assistant positions. T.L. and M.M. are indebted to the IWT-Flanders-Belgium for Ph.D. grants.

CM0112892

(50) Bosacek, V.; Dubinin, M. M.; Kadlets, O.; Murdmaa, K. O.; Navratil, V. *Dokl. Chem.* **1967**, *174*, 305.

(51) Gregg, S. J.; Langford, J. F. J. *Chem. Soc., Faraday Trans.* **1977**, *73*, 747.